

Journal of Materials Chemistry C

Accepted Manuscript



This is an *Accepted Manuscript*, which has been through the Royal Society of Chemistry peer review process and has been accepted for publication.

Accepted Manuscripts are published online shortly after acceptance, before technical editing, formatting and proof reading. Using this free service, authors can make their results available to the community, in citable form, before we publish the edited article. We will replace this *Accepted Manuscript* with the edited and formatted *Advance Article* as soon as it is available.

You can find more information about *Accepted Manuscripts* in the [Information for Authors](#).

Please note that technical editing may introduce minor changes to the text and/or graphics, which may alter content. The journal's standard [Terms & Conditions](#) and the [Ethical guidelines](#) still apply. In no event shall the Royal Society of Chemistry be held responsible for any errors or omissions in this *Accepted Manuscript* or any consequences arising from the use of any information it contains.

**Broadly Tuning Bi³⁺ Emission via Crystal Field Modulation in Solid Solution Compounds
(Y,Lu,Sc)VO₄:Bi for Ultraviolet Converted White LEDs**

Fengwen Kang,^a Mingying Peng,^{*a} Xiaobao Yang,^a Guoping Dong,^a Guochao Nie,^b Weijiang Liang,^b Shanhui Xu^a and Jianrong Qiu^a

^aThe State Key Laboratory of Luminescent Materials and Devices, the China-Germany Research Center for Photonic Materials and Devices, and the Institute of Optical Communication Materials, School of Materials Science and Engineering, South China University of Technology, Guangzhou 510641, China

^bNano Medicine Center, Yulin Normal University, Guangxi 537000, China

Abstract

For phosphor-converted white LEDs (pc-WLEDs) based on UV chips, it is essential to search high efficient phosphors that better feature with broadly tunable emission and particular have no or less excitation in visible ranges. This could allow the designer of pc-WLEDs to select the desirable emission wavelength and, thereby, fabricate the device with comfortable color perception. Conventional rare earth scheme, for instance Ce³⁺ or Eu²⁺ doped phosphors, can be tuned in emission wavelengths, but they cannot overcome the severe intrinsic excitation in the range from blue to green. We report here that Bi³⁺, the valence of which is confirmed by X-ray photoelectron (XPS) spectrum, can exhibit almost no excitation in the visible range and an extremely broad emission covering the full visible spectral range with internal quantum efficiency up to 75% once substituted into the solid solution compounds (Y,Lu,Sc)VO₄:Bi. When crystal field around Bi³⁺ is tuned by gradual substitution of smaller lanthanide ion for larger lanthanide ion in the solid solution, the emission peak position can be modulated linearly between 566 nm and 635 nm due to the susceptibility of bismuth naked 6s electrons to local environment. In accordance with Rietveld refining results, static and transient photoluminescence (PL) spectra reveal the existence of single type of Bi³⁺ emission center in the sample, to which energy transfer happens from VO₄³⁻ group to Bi³⁺ upon excitation into the charge transfer state of VO₄³⁻ groups. The mechanism of concentration quenching of Bi³⁺ emission is testified possibly due to dipole–quadrupole rather than exchange interactions. This work shows the potential application of bismuth doped samples in UV converted pc-WLEDs.

***Corresponding author.**

Tel: +86 20 87114204;

Fax: +86 20 22236910.

Email address: pengmingying@scut.edu.cn

1. Introduction

In recent years, considerable attentions have been paid to white light emitting diodes (WLEDs) primarily because of the overwhelming advantages such as higher luminous efficiency and brightness, lower power consumption, longer lifetime, smaller size *etc*, especially as compared to traditional incandescent and fluorescent lightings [1-5]. Hence, they have been coined as the ideal light source for next generation lighting and display industries. Pc-WLEDs is one of approaches to generate white lights on the basis of LEDs, and it usually combines one LED chip to one or multiple phosphors [6-7]. The main stream commercial technique of pc-WLEDs is to cover a blue LED chip with a yellow phosphor YAG:Ce, which is dispersed homogeneously into transparent hosts like either silicon or epoxy resin. For the design, the innate deficiency in red components leads to the unavoidable problems such as harsh light to human eyes due to high color temperature (CT), poor color rendering index (CRI) or low stability of CT under different driving currents [1-5]. These can be optimized in an alternative technique, which employs a composite of an UV chip with tri-color phosphors (namely, red, green and blue phosphors). This is called UV-pc-WLED, hereafter, and it has been considered as the promising direction of future solid state lighting because of obvious improvements in CRI and efficiency as well as tunable CT. In 2020, given the increased efficiency and the continuous government influences, it will be expected to become price competitive to fluorescent lamps and perhaps dominate the market of general illumination. The bottleneck is lack of efficient phosphors especially excitable only by near UV lights rather than blue to green lights. The phosphors are better tunable in emission wavelengths since it will increase the flexibility of wavelength selection, and therefore, allow designing the device of WLED with desirable quality of illumination, for instance, warm color perception.

Motivated by the idea, extensive efforts have been made previously, and they have led to the discovery of a series of efficient phosphors, for example Eu^{2+} doped nitride red phosphors [8-10]. There are also reports on Eu^{2+} or Ce^{3+} doped phosphors with tunable emissions. The color tuning of emission originates from the nature of the transitions from 5d to 4f since they are sensitive to the changes of surroundings. So the tuning could be made by tailoring the crystal field or bond covalence around Eu^{2+} or Ce^{3+} . For instance, increasing the content Sr_3SiO_5 in the solid solution between Sr_3SiO_5 and $\text{Sr}_3\text{AlO}_4\text{F}$ can result in an increase of lattice covalency, and it, thereby, leads to the redshift of Ce^{3+} emission from 474 nm to 537 nm [11]. Similar phenomena also appear in Eu^{2+} doped solid solution compounds, e.g. $\text{Sr}_{1.97-x}\text{Ca}_x\text{MgSi}_2\text{O}_7:\text{Eu},\text{Dy}$ [12]. Besides these, there are also strategies for tuning emission of phosphors, for instance, to choose double or even multiple types of activator ions which share common excitation wavelengths in near UV range or could transfer the absorbed energy from one to the other. Careful control over the energy transfer between them could as wished modulate the emission color of phosphor, for example, $(\text{Gd}-\text{Y}-\text{Bi}-\text{Eu})\text{VO}_4$ [13] or $\text{YAG}:\text{Ce}^{3+},\text{Mn}^{2+},\text{Si}^{4+}$ [14]. Nevertheless, all efforts have been concentrated mainly on the dopant schemes of either rare earth or transition metal. Their strong excitation in blue to green range could result in unavoidably reabsorption of just produced white light and hence the easy distortion of the required color quality, the luminous intensity and color

coordination of pc-WLED.

Non-rare-earth element of bismuth once substituted in a valence of +3 can exhibit emission in UV, blue, green or yellow, which depends on the exact type of host Bi^{3+} could be fitted into [15-16]. The adjustability of the emission stems from the susceptibility of naked bismuth 6s electrons to the surrounding field. Very recently, it was found even in a single compound of CaMoO_4 the emission of Bi^{3+} can be modulated from 554 nm to 586 nm when the microenvironment was tiny modified around Bi^{3+} by intentional introduction of alkali ions in the neighborhood [15]. These works prove at least partially that it is possible to manipulate the bismuth emission through composition design. However, so far, there are few reports on tunable emission of Bi^{3+} in solid solution compound.

As proof of concept, a set of orthovanadate compounds LnVO_4 ($\text{Ln}=\text{Y},\text{Lu},\text{Sc}$) has been selected in this paper as the playground to demonstrate the Bi^{3+} emission modulation via the control over the crystal field by composition. We choose these compounds because: (1) they are excellent hosts for trivalent activators, such as Eu^{3+} or Nd^{3+} , as noticed by Levine and Palilla [17], chemically and thermally stable and benign to environment [18]; (2) they crystallize in tetragonal space group $I4_1/amd$ with same identified crystallographic structure of zircon, which allows the formation of solid solution between each other [19-21]; (3) in which there are only one type of Ln^{3+} , V^{5+} and O^{2-} , which definitely could simplify the study on the interactions between activators and/or hosts; (4) The size and charge of Ln^{3+} are both comparable to Bi^{3+} , which would drive Bi^{3+} preferentially to occupy Ln^{3+} rather than V^{5+} , as depicted as **Fig.1 (a)**; (5) LnO_8 polyhedra are linked up with each other by sharing either edges or oxygen atoms; so once Bi^{3+} is substituted for Ln^{3+} shown in **Fig.1 (a)**, it can sense directly the slight changes in the nearest neighborhood (a radius of 3.84~5.85 Å around Bi^{3+}); (6) gradual decrease in ionic radius from eight-fold Y^{3+} (1.019 Å) to Lu^{3+} (0.977 Å) and then to Sc^{3+} (0.870 Å) will permit tailoring the lattice cell on the basis of the Végard law, and hence the crystal field around Bi^{3+} . Experiments turn out in this work indeed that the Bi^{3+} emission can be modulated in an unexpectedly wide spectral range, that is, from 566 nm to 635 nm. Surprisingly, the emission of the solid solution compounds $(\text{Y}_x,\text{Lu}_y,\text{Sc}_z)_{1-a}\text{VO}_4:a\text{Bi}$ spans the whole visible spectral range with the maximum quantum efficiency (QE) up to 75%. And it has almost no excitation in the visible range (>400 nm), which is distinguished from any rare earth or transition metal doped phosphor. Static and dynamic photoluminescence spectra and Rietveld refining as well as X-ray photoelectron spectrum have been used to comprehensively understand the complex luminescence dynamic of bismuth ion and the interactions between bismuth ions and/or hosts.

2. Experimental

2.1 Sample synthesis

All the solid solution samples of $(\text{Y}_x,\text{Lu}_y,\text{Sc}_z)_{1-a}\text{VO}_4:a\text{Bi}$ ($a=2.0\%$), where the sum of x , y and z keeps 1.0 in this work, were synthesized by the conventional solid state reactions at high temperature in air. Lu_2O_3 (99.99%), Y_2O_3 (99.99%), Sc_2O_3 (99.99%), NH_4VO_3 (99.9%) and Bi_2O_3 (99.999%) were selected as starting materials and weighed according to the nominal composition

$(Y_x, Lu_y, Sc_z)_{1-a}VO_4:aBi$. After thorough grinding for 2 hours in an agate mortar, the mixtures were moved into alumina crucibles, and sintered twice at 1100 °C for 3 hours with a heating rate of 3 °C/min and an intermediate grinding to further improve the homogeneity. The samples, afterwards, were kept in electric furnace and cooled to room temperature naturally. The final products were ground once again for consequent measurements. To define the optimal content of bismuth, we first change x gradually between 0 and 0.05 while keeping other elements constant. It is, therefore, determined to be 2.0% for $LuVO_4:Bi$ and $YVO_4:Bi$. Consequently, we fix the bismuth content as 2.0% and change the contents of Lu or Sc regularly between 0 and 1.0 to testify our concept of tuning the Bi^{3+} emission via systematic changes of local crystal field.

2.2 Characterization

The phase purity of all samples was examined with a Rigaku D/max-III A diffractometer with a $Cu K_\alpha$ radiation ($\lambda=1.5418 \text{ \AA}$), tube voltage and current set as 40 kV and 40 mA, respectively. Data were collected in a 2θ range from 10 to 90° with a scanning rate of 0.2° per second. Photoluminescence (PL, hereafter) spectra, quantum efficiency (QE, hereafter), decay curves and time-resolved PL spectra were measured with a high resolution Edinburgh Instruments FLS 920 spectrofluorometer equipped with a red-sensitive photomultiplier (Hamamatsu R928P) in a Peltier-cooled housing in the single photon counting mode and a closed cycle helium cryostat. Excitation curves were corrected over the lamp intensity with a silicon photodiode, and the emission curves were corrected by the detector spectral response. All measurements were performed at room temperature. X-ray photoelectron spectra (XPS) were measured using a Kratos Axis Ultra DLD spectrometer (Kratos Analytical Ltd., Wharfside, Manchester) with a focused monochromatic Al $K\alpha$ X-ray beam (1486.6 eV, 10 mA×12 kV, 5×10^{-9} torr), and the binding energies have been calibrated by the reference peak of C 1s at 284.6 eV.

3. Results and discussion

3.1 Crystal structure analysis

Analysis on X-Ray diffraction (XRD) spectra reveals all the samples appear as pure single phase. **Fig.1 (b)** exemplarily shows the XRD pattern of $(Y_0Lu_{1.0}Sc_0)_{0.98}VO_4:2.0\%Bi$ along with classic Rietveld refining results. The refining was performed with FullProf Suite Program, and it starts with the crystallographic data of $LuVO_4$ from Inorganic Crystal Structure Database (ICSD) Card No. 78083, and it converges with profile factor $R_p=5.99\%$, weighted profile factor $R_{wp}=7.84\%$, expected weighted profile factor $R_{exp}=5.27\%$, Bragg factor $R_{Bragg}=2.40\%$, crystallographic factor $R_F=1.87\%$ and indicator of goodness of fit $GOF=2.21$. The comparison between experimental and calculated results confirms that the sample can crystallize in the tetragonal $I4_1/amd$ space group (see **Fig.1 (b)**). The refining calculation produces lattice parameters of $a=7.0256 \text{ \AA}$, $c=6.2351 \text{ \AA}$, $V=307.7585 \text{ \AA}^3$ (see **Table 1**), slightly larger than $a=7.0254 \text{ \AA}$, $c=6.2347 \text{ \AA}$, $V=307.72 \text{ \AA}^3$ for the blank crystal of $LuVO_4$ (ICSD#78083). This is due to substitution of Lu^{3+} ($R_{Lu, CN=8}=0.977 \text{ \AA}$, where CN stands for coordination number) with larger Bi^{3+} ($R_{Bi, CN=8}=1.17 \text{ \AA}$). **Fig.1 (c)** illustrates the XRD patterns of $(Y_x, Lu_y, Sc_z)_{0.98}VO_4:0.02Bi$, where x , y , or z varies between 0 and 1.0. All the diffraction peaks can be indexed in the same space group as $LuVO_4$, meaning formation of solid

solution as expected. When x keeps constant, all diffraction peaks shift towards higher angle side as y or z increases in sequence. This could be more manifested in **Fig.1 (d)**, where the plane (200) moves to higher angle from bottom to top. It implies the regular shrinkage of lattice cell according to Bragg's law ($n\lambda=2d\sin\theta$, where n is an integer, λ is the wavelength of incident X-ray, d is the spacing between the planes in the atomic lattice, and θ is the angle between the incident ray and the scattering planes.), and it agrees well with the refining results listed in **Table 1**. And lattice parameters a , c and V decrease according to Vegard law.

The refined results reveal that there is one type of Ln^{3+} ions in $\text{LnVO}_4:2.0\%\text{Bi}$ ($\text{Ln}=\text{Y, Lu, Sc}$), which Bi^{3+} prefers substitution for. And they are coordinated by eight oxygen atoms with two different bond lengths, as depicted in **Fig.1 (e)**. The average length of Ln-O is 2.3644 Å for $\text{YVO}_4:2.0\%\text{Bi}$, 2.3394 Å for $\text{LuVO}_4:2.0\%\text{Bi}$, and 2.2333 Å for $\text{ScVO}_4:2.0\%\text{Bi}$. And the regular decrease in sequence of $\text{Y}\rightarrow\text{Lu}\rightarrow\text{Sc}$ allows control over the crystal field around Ln ions by variation of composition.

3.2 Identification of bismuth valence in doped samples

Bismuth, when introduced into solid samples at higher temperature, could readily transform into different valence states, and even aggregate into small entities such as homonuclear clusters, for instance Bi_5^{3+} [22-23]. And it is able to luminescence in ultraviolet, visible, near infrared, or even mid infrared at room temperature, which tightly depends on the exact species bismuth could be stabilized in solids [16, 24]. So, in order to understand the intriguing nature of bismuth luminescence, it is highly essential to identify the valence of bismuth in the samples. Therefore, we checked over every sample of $(\text{Y}_x\text{Lu}_y\text{Sc}_z)_{1-a}\text{VO}_4:a\text{Bi}$ with XPS spectrum, and these spectra appear very similar. So we listed the spectra of $\text{Y}_{0.98}\text{VO}_4:2.0\%\text{Bi}$, $\text{Lu}_{0.98}\text{VO}_4:2.0\%\text{Bi}$ and $\text{Sc}_{0.98}\text{VO}_4:1.0\%\text{Bi}$ for example in **Fig.2**. $\alpha\text{-Bi}_2\text{O}_3$ was used as reference sample for trivalent bismuth of Bi^{3+} . Comparison of our samples to $\alpha\text{-Bi}_2\text{O}_3$ shows that trivalent bismuth dominates in all samples, as reflected by characteristics peaks of Bi^{3+} at ~ 159.3 eV ($4f_{7/2}$) and 164.6 eV ($4f_{5/2}$), respectively (see **Fig.2**). This agrees with that reported by Zhang *et al* [25].

3.3 Photoluminescence (PL) analysis

The blank samples of $(\text{Y}_x\text{Lu}_y\text{Sc}_z)_{1-a}\text{VO}_4:a\text{Bi}$ ($a=0$) exhibit blue emission of VO_4^{3-} groups due to the transition from ${}^1\text{B}({}^1\text{T}_2)$ to the ground state ${}^1\text{A}_1$ upon excitation of UV for instance at 265 nm. And it shifts red regularly along the radius decrease of lanthanide ion, that is, from 435 nm for YVO_4 , to 440 nm for LuVO_4 and to 465 nm for ScVO_4 . Two excitation peaks were found at ~ 260 nm and ~ 320 nm in blank sample of YVO_4 , and they correspond to ${}^1\text{A}_1\rightarrow{}^1\text{E}({}^1\text{T}_1)$ and ${}^1\text{A}_1\rightarrow{}^1\text{B}({}^1\text{T}_2)$, respectively. The longer wavelength peak shifts red to ~ 330 nm for sample ScVO_4 . Once bismuth was introduced into the samples, the samples become light brown (see the inset of **Fig.4 (a)**), and the excitation peaks are broadened particularly at longer wavelength region due to superimposition of bismuth excitation peak (${}^1\text{S}_0\rightarrow{}^3\text{P}_1$) (see **Fig.3**). For instance, the tail of excitation of YVO_4 stops around 360 nm, while $\text{Y}_{0.98}\text{VO}_4:2.0\%\text{Bi}$ extends to ~ 380 nm. As inspecting **Fig.3** from bottom to top, that is, along with the decrease of lattice parameters, the tail of excitation peak of bismuth moves continuously to ~ 430 nm from ~ 380 nm.

Similar scenario happens to the emission peak. **Figure 4 (a)** depicts the emission spectra of solid solution compounds $(Y_x, Lu_y, Sc_z)_{1-a}VO_4:aBi$, where x , y , or z changes between 0 and 1.0, respectively, and a value is equal to 0.02. Upon excitation into the charge transfer state of the VO_4^{3-} groups, for instance by 254 nm, the samples emit brilliant yellow, orange, or even red lights (see the inset of **Fig.4 (a)**). **Fig.4 (a)** illustrates exactly how the emission color changes with sample. All samples show the ultrabroad emission spanning the full visible spectral range (400-760 nm), to which none of any rare earth doped phosphors can so far be comparable. A full width at half maximum (FWHM) of the emissions is larger than 160 nm. The feature of broadband seems unique for bismuth doped photonic materials. For instance, we found bismuth doped glasses even glow the near infrared spectra ranging from 1000 nm to 1700 nm with FWHM larger than 400 nm [26-27]. As the content y of Lu increases from 0 to 1, the emission peak shifts from 566 nm to 576 nm, which continues to 635 nm when the content z of Sc increases gradually to 1. As plotting the peak position of emission against y or z , we found they well fit linear equation $m=a+kn$ as shown in **Fig.4 (b)**. For instance, the experimental emission peaks at ~ 601 nm for $z=0.4$ and the fitted value is 601.03 nm. They consist with each other very well. Corresponding CIE chromaticity coordinates of the solid-solution compounds are listed in **Table 1**, and representative CIE chromaticity coordinates are plotted in **Fig.4 (c)**. This vividly illustrates that the emission color can be tuned from yellow (0.419, 0.489) to red (0.522, 0.431), and the emission of Bi^{3+} can be manipulated desirably peaking in the range of 566-635 nm. Hence, the manipulation can be achieved by simply selecting a proper ratio of Lu/Y and Sc/Lu in solid solution compounds $(Y_x, Lu_y, Sc_z)_{1-a}VO_4:aBi$.

3.4 Discussions on the tunable emissions

The luminescence of Bi^{3+} is very complicated itself, and it can emit in a wide spectral range from UV to yellow or even red in this work. Even when doped into the compounds which share same crystal structure, for instance Bi^{3+} doped scheelite-structured $CaWO_4$ and $CaMoO_4$ [15, 24], it behaviors very differently. As the excitation wavelength changes from 250 nm to 300 nm, sample emission only red shifts in $CaWO_4:Bi^{3+}$, while in $CaMoO_4:Bi^{3+}$, the initial red shifts of the emission is followed tightly by the blue shifts. At first glance, tunable emission of Bi^{3+} in solid solution compounds $(Y_x, Lu_y, Sc_z)_{1-a}VO_4:aBi$ intuitively correlates to contraction of lattice volumes, as shown in **Fig.4 (d)**. As the atom number per cell keeps constant, the decrease of lattice volume means the shortening of distance between atoms, as exemplarily illustrated in **Fig.1 (e)**. This enhances the interaction between atoms, so Bi^{3+} will experience a stronger crystal field as the content of Lu or Sc increases in turn. This will gradually lower the excited state 3P_1 and therefore lead to the regular red shifts of the emission and the excitation edge.

The distance reduction between atoms also means the increase of bond covalence. To quantify the covalency of lanthanon (Ln) to oxygen bond and try to reveal its underlying relationship to the emission, we calculated the chemical bond covalencies (f_c) for Ln-O in the solid solution by the dielectric chemical bond theory of complex ionic crystals on the basis of the Rietveld refined crystallographic data. **Fig.5** illustrates the average covalence f_c of Ln-O against emission peaks.

And it indicates that the increase of f_c basically leads to the red shifts of Bi^{3+} emission. A linear equation ($y=0.1259+5.176\times 10^{-5}x$) can be established between them, as depicted in **Fig.5**. This implies again the sensitivity of Bi^{3+} to surrounding environment, and it governs the tunability of Bi^{3+} emission.

For practical application in WLEDs, QE of solid solution compounds $(\text{Y}_x\text{Lu}_y\text{Sc}_z)_{1-a}\text{VO}_4:\text{aBi}$ should be considered. The Edinburgh Instruments FLS 920 spectrofluorometer equipped with an integration sphere is not applicable to excitation wavelength shorter than 300 nm when measuring QE. We, therefore, measured QE upon the excitation at 330 nm rather than 265 nm or 254 nm. We selected this wavelength also because the excitation intensity at 330 nm is comparable to the latter two. The results are included in **Table 2**, and they show the internal QE is 75% for $\text{YVO}_4:2.0\%\text{Bi}^{3+}$, 68% for $\text{LuVO}_4:2.0\%\text{Bi}^{3+}$ and 35% for $\text{ScVO}_4:2.0\%\text{Bi}^{3+}$. The decrease of QE with the emission peak is due to the increase of quantum defect. The high QE and the absence of excitation in visible range shown in **Fig.3** imply the promising application of $(\text{Y}_x\text{Lu}_y\text{Sc}_z)_{1-a}\text{VO}_4:\text{aBi}$ in UV-pc-WLED. When applied in UV-pc-WLED, these phosphors can well avoid the reabsorption of the produced white light, to which none of present rare earth doped yellow or red phosphor can be comparable.

3.5 Energy transfer in bismuth doped solid solution

According to Rietveld refining results, there is only one type of Ln coordinated by eight oxygen atoms in bismuth doped solid solution, which lattice site bismuth prefers to occupy in view of matches of both size and charge. This consists with time resolved emission spectra of $(\text{Y}_x\text{Lu}_y\text{Sc}_z)_{1-a}\text{VO}_4:\text{aBi}$. Since these spectra are very similar, only exemplary spectra of $\text{LuVO}_4:2.0\%\text{Bi}^{3+}$ (see **Fig.6**), which corresponds to $x=0, y=1, z=0$ and $a=0.02$ in the solid solution. As illustrated in **Fig.6**, with the delay prolonged, the intensity of the Bi^{3+} emission gradually decreases while the spectrum feature keeps unchanged. For instance, the peak position is always located at ~ 576 nm. Similarly, the emission peak keeps at 566 nm for $\text{YVO}_4:2.0\%\text{Bi}^{3+}$, and 635 nm for $\text{ScVO}_4:2.0\%\text{Bi}^{3+}$, which correspond to $x=1, y=0, z=0, a=0.02$ and $x=0, y=0, z=1, a=0.02$ in $(\text{Y}_x\text{Lu}_y\text{Sc}_z)_{1-a}\text{VO}_4:\text{aBi}$, respectively. These reveal that there is only one type of Bi emission center in bismuth doped solid solution compounds of $(\text{Y}_x\text{Lu}_y\text{Sc}_z)_{1-a}\text{VO}_4:\text{aBi}$.

Figure 7 depicts the dependence of emission spectrum of bismuth doped LuVO_4 on bismuth concentration. As bismuth is doped into the compound, the broad Bi^{3+} emission at round 576 nm instantly appears while typical emission of VO_4^{3-} groups at 440 nm gradually diminishes. As the bismuth content continues increasing, the emission intensity initially increases, reaches the maximum at 2.0%Bi, and decreases afterwards. The emission peak location keeps fixed all the way. This is the typical concentration quenching effect. Since excitation into the absorption of VO_4^{3-} groups always leads to the apparition of the Bi^{3+} emission, and also the emission of Bi^{3+} is intensified at the expense of the emission of VO_4^{3-} groups, there must be an energy transfer from VO_4^{3-} groups to Bi^{3+} . Inspecting **Fig.3** and **Fig.7** reveals to us that there is an overlap between emission band of VO_4^{3-} groups and the excitation band of Bi^{3+} . This provides a path to transfer energy from VO_4^{3-} groups to Bi^{3+} . It can be a process of radiation of the VO_4^{3-} groups followed by

reabsorption of Bi^{3+} , or perhaps a resonant nonradiative transfer between them since these luminophors share common excitation in UV spectral range.

In order to testify the energy transfer from the VO_4^{3-} groups to Bi^{3+} , the decay curves of $\text{LuVO}_4:\text{xBi}^{3+}$ ($\text{x}=0, 0.5\%, 1.0\%, 2.0\%, 3.0\%$ and 5.0%) samples were measured upon the excitation of 265 nm while monitored at the emission of 440 nm, and listed as **Fig.8**. All decay curves can be fitted by the single exponential decay equation as follows [6, 28]:

$$I(t)=A\exp(-t/\tau) \quad (1)$$

where τ is the decay component, parameter A is the fitting constant. Fitting with equation (1) produces the VO_4^{3-} lifetimes of 9.89 μs , 9.54 μs , 8.76 μs , 7.91 μs , 7.74 μs and 7.21 μs , corresponding to the content of bismuth 0, 0.5%, 1.0%, 2.0%, 3.0% and 5.0%, respectively (see **curve 1** in **Fig.8 (b)**). The decrease of the VO_4^{3-} lifetimes demonstrates the energy transfer from VO_4^{3-} groups to Bi^{3+} . The energy transfer efficiency (η_T) from VO_4^{3-} groups to Bi^{3+} can be evaluated with the following expression [6, 28]:

$$\eta_T=1-\tau_s/\tau_{s0} \quad (2)$$

where τ_{s0} and τ_s parameters represent the lifetime of VO_4^{3-} groups in the absence and the presence of Bi^{3+} , respectively. η_T is, thus, estimated to be 3.5%, 11.4%, 20.1%, 21.7% and 27.1% for the content of bismuth 0, 0.5%, 1.0%, 2.0%, 3.0% and 5.0%, respectively (see **curve 2** in **Fig.8 (b)**). This indicates that the energy transfer efficiency (η_T) increases with the Bi^{3+} content and it reaches the maximum value (27.1%) at the Bi^{3+} concentration of 5.0%. At high concentration of Bi^{3+} , it becomes harder to distinguish the emission at 440 nm from VO_4^{3-} groups or Bi^{3+} since they overlap each other at the wavelength. The lifetime of the VO_4^{3-} groups should be much lower than the measured value at higher content of bismuth. And it means a higher efficiency of energy transfer happening from VO_4^{3-} groups to Bi^{3+} than calculated. This could be witnessed by the disappearance of the VO_4^{3-} emission at higher bismuth content (see **Fig.7**).

As shown in **Fig.7**, the critical Bi concentration is 2.0%. So, the critical distance R_c for the energy transfer in $\text{LuVO}_4:\text{Bi}^{3+}$ can be calculated with the formula [6, 28-29]:

$$R_c = \sqrt[3]{6V / (\pi x_c N)} \quad (3)$$

, where x_c is the critical concentration of Bi^{3+} , N is the number of total Lu lattice sites in unit cell which are supposed to be substituted by Bi^{3+} , and V represents the cell volume. In this work, for $x_c=0.02$, $N=4$, and $V=307.7585 \text{ \AA}^3$ (see **Table 1**), combining equation (3) produces $R_c=19.44 \text{ \AA}$. Similarly, as x_c equals 0.02 in $\text{YVO}_4:\text{Bi}$ and 0.01 in $\text{ScVO}_4:\text{Bi}$, the critical distances (R_c) are evaluated to be 19.68 \AA and 23.82 \AA for these compounds, respectively.

Exchange and multipolar interactions are known as two types of the resonant energy transfer progresses. In general, if the exchange interaction dominated an energy transfer, it restricts the critical distance between the sensitizer and activator to 5-8 \AA [29]. It is obviously not the case in bismuth doped solid solution of $(\text{Y}_x,\text{Lu}_y,\text{Sc}_z)_{1-a}\text{VO}_4:\text{aBi}$. The values of R_c are rather large for exchange interactions, so this implies the multipolar interaction as the dominant mechanism in concentration quenching in bismuth doped samples. At the higher Bi^{3+} concentration,

non-radiative energy migration will be enhanced according to the Dexter's energy transfer theory, and it therefore leads to quenching of emission.

The potential multipolar energy transfer mechanism can be analyzed with the equation proposed by Van Uitert [30]:

$$I/x = k/(1 + \beta(x/x_c')^{\theta/3}) \quad (4)$$

, where I is the emission intensity at 576 nm for concentration x ; x_c' is the critical concentration; k and β are constants for specific interaction in the host; and θ could be 6, 8, or 10, which corresponds to the dipole-dipole ($d-d$), dipole-quadrupole ($d-q$) and quadrupole-quadrupole ($q-q$) interaction, respectively. $\ln(I/x)$ was plotted against $\ln(x/x_c')$ in **Fig.9**. Best consistence was found for $\theta=8$ with $\gamma^2=99.61\%$, which means the $d-q$ interaction is responsible for the energy transfer mechanism. The same mechanism also goes to bismuth doped solid solution compounds, for instance $\text{YVO}_4:\text{Bi}^{3+}$ and $\text{ScVO}_4:\text{Bi}^{3+}$.

4. Conclusions

In this work, a series of Bi^{3+} doped solid solution compounds of $(\text{Y}_x\text{Lu}_y\text{Sc}_z)_{1-a}\text{VO}_4:a\text{Bi}$ were successfully synthesized by solid state reaction at high temperature. They show a superbroad emission covering the whole visible spectrum and almost no excitation at wavelength longer than 400 nm, to which none of phosphors based on rare earth scheme can be comparable due to limitation of their intrinsic nature of the transitions. The emission of Bi^{3+} can be tuned in a wide spectral range from 566 nm to 635 nm on the basis of linear relationship between the position of emission peak and the average covalency f_c of Ln-O bond, which can be evaluated by the dielectric chemical bond theory of complex ionic crystals. The continuous emission tuning can be realized by simple variation of composition of the solid solution, and it, therefore, allows designing the phosphor with desirable emission wavelength in the range. Energy transfer did happen from VO_4^{3-} groups to Bi^{3+} and the efficiency of the transfer increases along bismuth content. Analysis of the dependence of Bi^{3+} emission on concentration with the Van Uitert equation reveals that dipole-quadrupole rather than exchange interaction dominates the quenching. The widely tunable emission with a high QE up to 75% suggests the Bi^{3+} doped solid solution phosphors a very promising candidate in UV-pc-WLED.

Acknowledgements

This work was financially supported by the National Natural Science Foundation of China (Grant Nos. 51322208, 51072060, 11174085, 11104080, 51302087, 51102096), Fundamental Research Funds for the Central Universities (Grant No.2013ZG004), Guangdong Natural Science Foundation for Distinguished Young Scholars (Grant No. S20120011380), Chinese Program for New Century Excellent Talents in University (Grant No. NCET-11-0158), the Department of Education of Guangdong Province (Grant No. 2013gjh0001) and Fok Ying Tong Education Foundation (Grant No. 132004).

References:

- [1] Li, X. F.; Budai, J. D.; Liu, F.; Howe, J. Y.; Zhang, J. H.; Wang, X. J.; Gu, Z. J.; Sun, C. J.; Meltzer, R. S.; Pan, Z. W. *Light: Science & Applications*, **2013**, 2, e50-E59.
- [2] Daicho, H.; Iwasaki, T.; Enomoto, K.; Sasaki, Y.; Maeno, Y.; Shinomiya, Y.; Aoyagi, S.; Nishibori, E.; Sakata, M.; Sawa, H.; Matsuishi, S.; Hosono, H. *Nat. Commun.*, **2012**, 3, 1132-1141.
- [3] Kasahara, T.; Aizawa, D.; Irikura, T.; Moriyama, T.; Toda, M.; Iwamoto, M. *J. Light Vis. Env.*, **2006**, 30, 95-103.
- [4] Hashimoto, T.; Wu, F.; Speck, J. S.; Nakamura, S. *Nat. Mater.*, **2007**, 6, 568-571.
- [5] Huang, K. W.; Chen, W. T.; Chu, C. I.; Hu, S. F.; Sheu, H. S.; Cheng, B. M.; Chen, J. M.; Liu, R. S. *Chem. Mater.*, **2012**, 24, 2220-2227.
- [6] Peng, M. Y.; Yin, X. W.; Tanner, P. A.; Liang, C. Q.; Li, P. F.; Zhang, Q. Y.; Qiu, J. R. *J. Am. Ceram. Soc.*, **2013**, 96, 2870-2876.
- [7] Li, P. F.; Peng, M. Y.; Yin, X. W.; Ma, Z. J.; Dong, G. P.; Zhang, Q. Y.; Qiu, J. R. *Opt. Express.*, **2013**, 18943-18948.
- [8] Hoppe, H. A.; Lutz, H.; Morys, P.; Schnick, W.; Seilmeier, A. *J. Phys. Chem. Solids.*, **2000**, 61, 2001-2006.
- [9] Li, Y. Q.; van Steen, J. E. K.; van Krevel, J. W. H.; Botton, G.; Delsing, A. C. A.; Disalvo, F. J.; de With, G.; Hintzen, H. T. *J. Alloy Compd.*, **2006**, 417, 273-279.
- [10] Xie, R. J.; Hirosaki, N.; Suehiro, T.; Xu, F. F.; Mitomo, M. *Chem. Mater.*, **2006**, 18, 5578-5583.
- [11] Im, W. B.; George, N.; Kurzman, J.; Brinkley, S.; Mikhailovsky, A.; Hu, J.; Chmelka, B. F.; Baars, S. P. D.; Seshadri, R. *Adv. Mater.*, **2011**, 23, 2300-2305.
- [12] Wu, H. Y.; Wang, Y. H.; Hu, Y. H.; Deng, L. Y.; Xie, W. *J. Phys. D: Appl. Phys.*, **2009**, 42, 125406-125412.
- [13] Chen, L.; Chen, K. J.; Hu, S. F.; Liu, R. S. *J. Mater. Chem.*, **2011**, 21, 3677-3685.
- [14] Jia, Y. C.; Huang, Y. J.; Zheng, Y. H.; Guo, N.; Qiao, H.; Zhao, Q.; Lv, W. Z.; You, H. P. *J. Mater. Chem.*, **2012**, 22, 15146-15152.
- [15] Kang, F. W.; Peng, M. Y.; Xu, S. H.; Ma, Z. J.; Dong, G. P.; Qiu, J. R. *Eur. J. Inorg. Chem.*, **2014**, 2014, 1373-1380.
- [16] Bountinaud, P. *Inorg. Chem.* **2013**, 52, 6028-6038.
- [17] Levine, A. K.; Palilla, F. C. *Appl. Phys. Lett.*, **1964**, 5, 118-120.
- [18] Li, Y.; Zheng, Y. H.; Wang, Q. M.; Zhang, C. C. *Mater. Chem. Phys.*, **2012**, 135, 451-456.
- [19] Cong, H. J.; Zhang, H. J.; Yao, B.; Yu, W. T.; Zhao, X.; Wang, J. Y.; Zhang, G. C. *Crystal Growth & Design*, **2010**, 10, 4389-4399.
- [20] Krumpel, A. H.; Kolk, E.; CaValli, E.; Boutinaud, P.; Bettinelli, M.; Dorenbos, P. *J. Phys.: Condens. Matter*, **2009**, 21, 115503-11511.
- [21] Blasse, G.; Brill, A. *J. Chem. Phys.*, **1969**, 50, 2974-2980.
- [22] Cao, R. P.; Peng, M. Y.; Zheng, J. Y.; Qiu, J. R.; Zhang, Q. Y. *Opt. Express.*, **2012**, 20(16),

18505-18514.

[23] Cao, R. P.; Peng, M. Y.; Wondraczek, L.; Qiu, J. R. *Opt. Express.*, **2012**, 20, 2562-2571.

[24] Kang, F. W.; Peng, M. Y. *Dalton Trans.*, **2014**, 43, 277-285.

[25] Zhang, Li.; Hashimoto, Y.; Taishi, T.; Nakamura, I.; Ni, Q. Q. *Appl. Surf. Sci.*, **2011**, 257, 6577-6582.

[26] Peng, M. Y.; Qiu, J. R.; Chen, D. P.; Meng, X. G.; Zhu, C. S. *Opt. Lett.*, **2004**, 29(17), 1998-2000.

[27] Peng, M. Y.; Qiu, J. R.; Chen, D. P.; Meng, X. G.; Zhu, C. S. *Opt. Lett.*, **2005**, 30(18), 2433-2435.

[28] Dai, P. P.; Zhang, X. T.; Bian, L. L.; Lu, S.; Liu, Y. C.; Wang, X. J. *J. Mater. Chem. C.*, **2013**, 1, 4570-4676.

[29] Blasse, G.; Grabmaier B. *Luminescent Materials.*, **1994**, Springer Verlag, Berlin, Heidelberg.

[30] Van Uitert, L.; *J. Electrochem. Soc.*, **1967**, 114(10), 1048-53.

Figure captions:

Fig.1 (a) Double lattice cell of LuVO_4 viewed along axis a , which is drawn on the basis of calculation results of Fig.1 (b); Bi^{3+} is exemplarily shown to substitute for Lu site; (b) XRD pattern (—) of $(\text{Y}_0\text{Lu}_{1.0}\text{Sc}_0)_{0.98}\text{VO}_4:2.0\%\text{Bi}$, Rietveld refining results (\bullet), Bragg reflections (\square) and the profile difference between experimental and calculated values (—); (c) XRD patterns of solid solution compounds $(\text{Y}_x\text{Lu}_y\text{Sc}_z)_{0.98}\text{VO}_4:2.0\%\text{Bi}$; for all samples in this work, $x+y+z=1$, and the specific values of x , y , and z are indicated in the formula beside each curve; (d) the zoom-in patterns of Fig.1 (c) in the range of $24.5\text{--}27^\circ$; (e) Changes of Ln-O bond lengths in dodecahedral $[\text{LnO}_8]$ structure, where Ln stands for Y, Lu and Sc, respectively.

Fig.2 XPS spectra of $\alpha\text{-Bi}_2\text{O}_3$ (black curve), $\text{Y}_{0.98}\text{VO}_4:2.0\%\text{Bi}^{3+}$ (red curve), $\text{Lu}_{0.98}\text{VO}_4:2.0\%\text{Bi}^{3+}$ (blue curve) and $\text{Sc}_{0.99}\text{VO}_4:1.0\%\text{Bi}^{3+}$ (violet curve).

Fig. 3 Excitation spectra of solid solution compounds $(\text{Y}_x\text{Lu}_y\text{Sc}_z)_{1-a}\text{VO}_4:a\text{Bi}$, where x , y , or z changes between 0 and 1.0, respectively, while a varies between 0 and 0.02. Monitored emission wavelengths are labeled beside each curve, and they correspond to the emission peak of each sample.

Fig. 4 (a) Emission spectra of solid solution compounds $(\text{Y}_x\text{Lu}_y\text{Sc}_z)_{1-a}\text{VO}_4:a\text{Bi}$, where x , y , or z changes between 0 and 1.0, respectively, while a equals 0.02, upon excitation into 265 nm; inset: digital photographs of corresponding samples exposed to natural lights (upper) and a UV lamp with a wavelength of 254 nm; (b) dependence of the emission positions on the ratios of Lu/Y and Sc/Lu, the fitted results is on the base of the equation $m=a+kn$; (c) CIE chromaticity coordinates of $(\text{Y}_x\text{Lu}_y\text{Sc}_z)_{1-a}\text{VO}_4:a\text{Bi}$ ($x=1, y=0, z=0, a=0.02$; $x=0.8, y=0.2, z=0, a=0.02$; $x=0, y=0.8, z=0.2, a=0.02$; $x=0, y=0.6, z=0.4, a=0.02$; $x=0, y=0.4, z=0.6, a=0.02$; $x=0, y=0, z=1, a=0.02$); (d) Relationship between the cell volumes (V) and the emission positions.

Fig. 5 Dependence of Bi^{3+} emission position on the average Ln-O covalency in the solid solution compounds. Red line is generated with the equation $y=0.1259+5.176\times 10^{-5}x$.

Fig. 6 Time-resolved spectra of $(\text{Y}_x\text{Lu}_y\text{Sc}_z)_{1-a}\text{VO}_4:a\text{Bi}$ ($x=0, y=1, z=0$ and $a=0.02$) sample upon excitation into 265 nm.

Fig.7 Emission spectra of $\text{LuVO}_4:a\text{Bi}^{3+}$ ($a=0, 0.5\%, 1.0\%, 2.0\%, 3.0\%$ and 5.0%) samples upon the excitation wavelength at 265 nm; Red dash line denotes disappearing of the VO_4^{3-} emission.

Fig.8 (a) Typical decay curve ($\lambda_{\text{ex}}=265\text{ nm}$, $\lambda_{\text{em}}=440\text{ nm}$) of $\text{LuVO}_4:2.0\%\text{Bi}^{3+}$ sample; the blue curve is fitted with the single decay equation $I(t)=A\exp(-t/\tau)$; (b) The dependence of the fitted lifetimes of VO_4^{3-} groups (curve 1) and energy transfer efficiencies (η_T) (curve 2) on Bi^{3+} concentration.

Fig.9 Dependence of $\ln(I/x)$ on (a) $\ln(x/x_c)^{6/3}$, (b) $\ln(x/x_c)^{8/3}$, and (c) $\ln(x/x_c)^{10/3}$ in $\text{LuVO}_4:a\text{Bi}$ ($a=0.5\%, 1.0\%, 2.0\%, 3.0\%$ and 5.0%). Correlation efficiencies are 97.29%, 99.61%, and 94.41% for the fittings in (a), (b) and (c), respectively.

Table 1. Lattice parameters (a and c in Å and V in Å³) and color coordinate (x, y) of solid solution compounds

Compounds	Lattice Parameter	Color coordinate	Lifetime (μs)
YVO ₄ :Bi	a=7.1239, c=6.2961, V=319.5317	(0.419, 0.489)	8.4
Y _{0.8} Lu _{0.2} VO ₄ :Bi	a=7.1099, c=6.2859, V=317.7556	(0.443, 0.484)	7.4
Y _{0.6} Lu _{0.4} VO ₄ :Bi	a=7.0820, c=6.2683, V=314.3857	(0.424, 0.472)	8.8
Y _{0.4} Lu _{0.6} VO ₄ :Bi	a=7.0561, c=6.2523, V=311.2951	(0.437, 0.476)	9.5
LuVO ₄ :Bi	a=7.0256, c=6.2351, V=307.7585	(0.444, 0.474)	7.3
Lu _{0.8} Sc _{0.2} VO ₄ :Bi	a=7.0023, c=6.2308, V=305.5076	(0.465, 0.474)	7.9
Lu _{0.6} Sc _{0.4} VO ₄ :Bi	a=6.9819, c=6.2299, V=304.1778	(0.487, 0.470)	8.1
Lu _{0.4} Sc _{0.6} VO ₄ :Bi	a=6.9343, c=6.2202, V=299.0948	(0.505, 0.461)	9.1
ScVO ₄ :Bi	a=6.7804, c=6.1345, V=282.7764	(0.522, 0.431)	5.4

Table 2. Bond Length *d* (Å) and quantum efficiency (QE) ($\lambda_{\text{ex}}=330$ nm) of LnVO₄:2.0%Bi³⁺ (Ln=Y, Lu, Sc) samples

Compounds	Bond	Bond Length <i>d</i> of ICSD Parameter	Present <i>d</i>	QE (%)
YVO ₄ :Bi	Y-O(1)x4	2.2980	2.2875	75
	Y-O(2)x4	2.4327 (ICSD#78074)	2.4412	
LuVO ₄ :Bi	Lu-O(1)x4	2.2516	2.2635	68
	Lu-O(2)x4	2.4100 (ICSD#78083)	2.4152	
ScVO ₄ :Bi	Sc-O(1)x4	2.1289	2.1155	35
	Sc-O(2)x4	2.3672 (ICSD#78073)	2.3507	

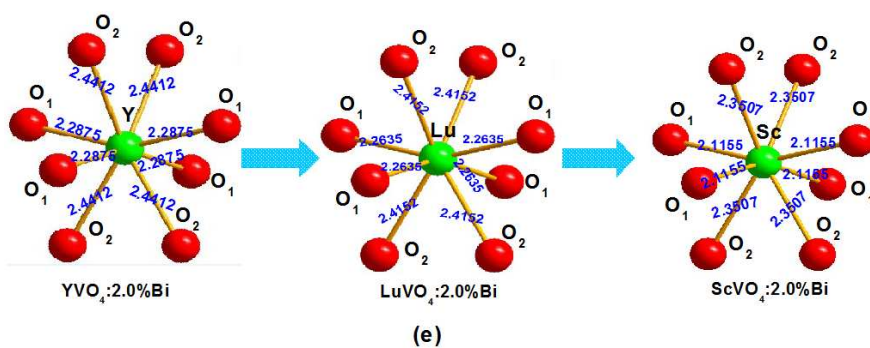
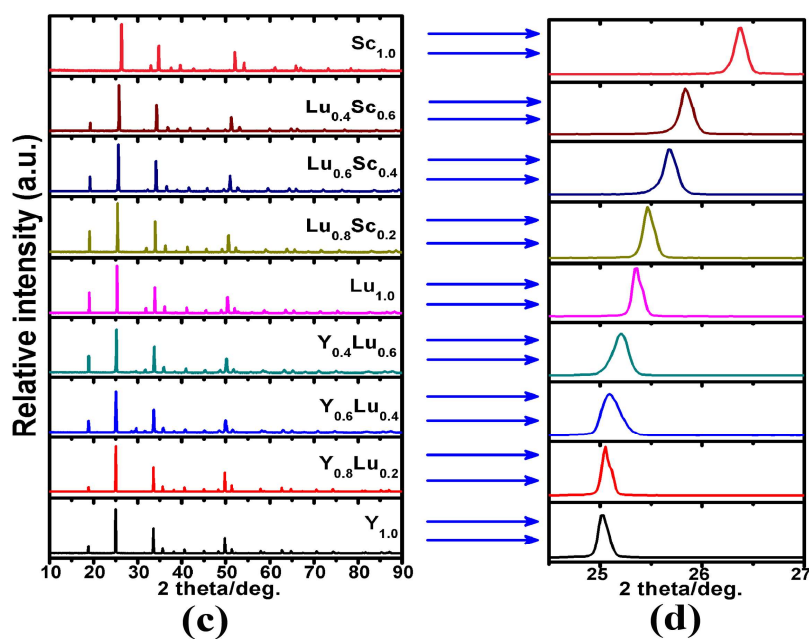
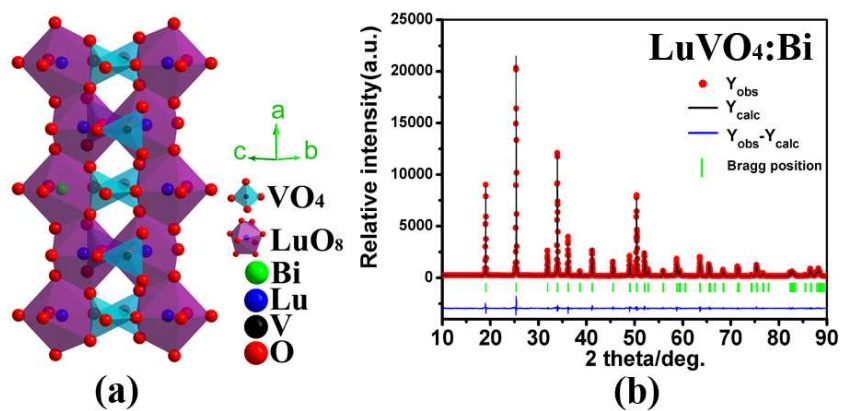


Fig.1

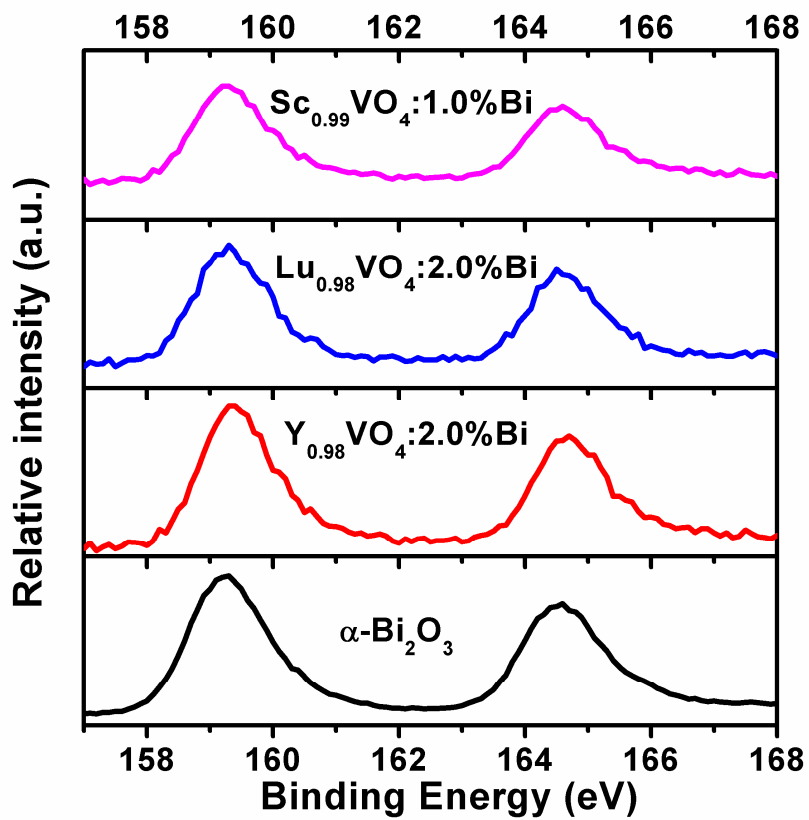


Fig. 2

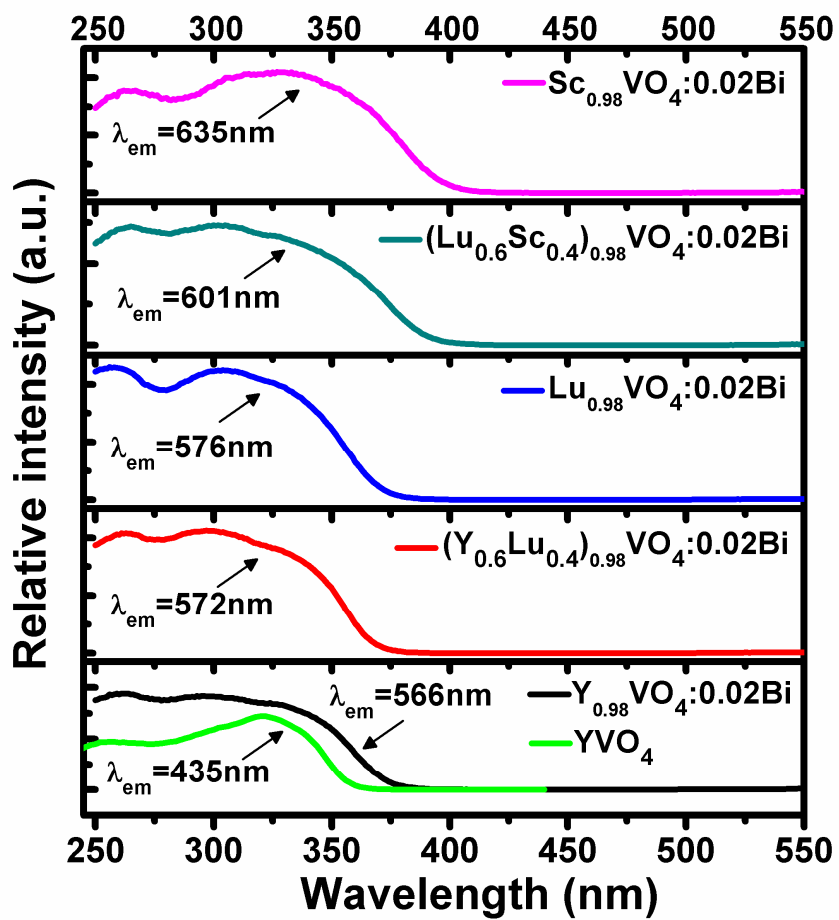


Fig.3

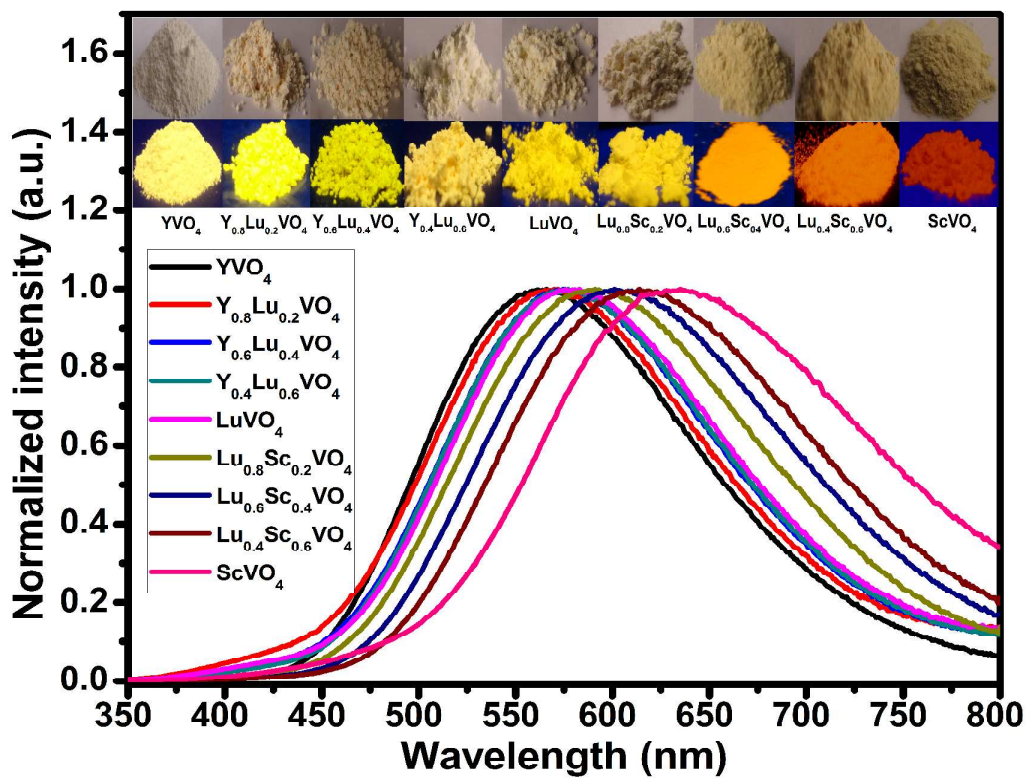


Fig. 4 (a)

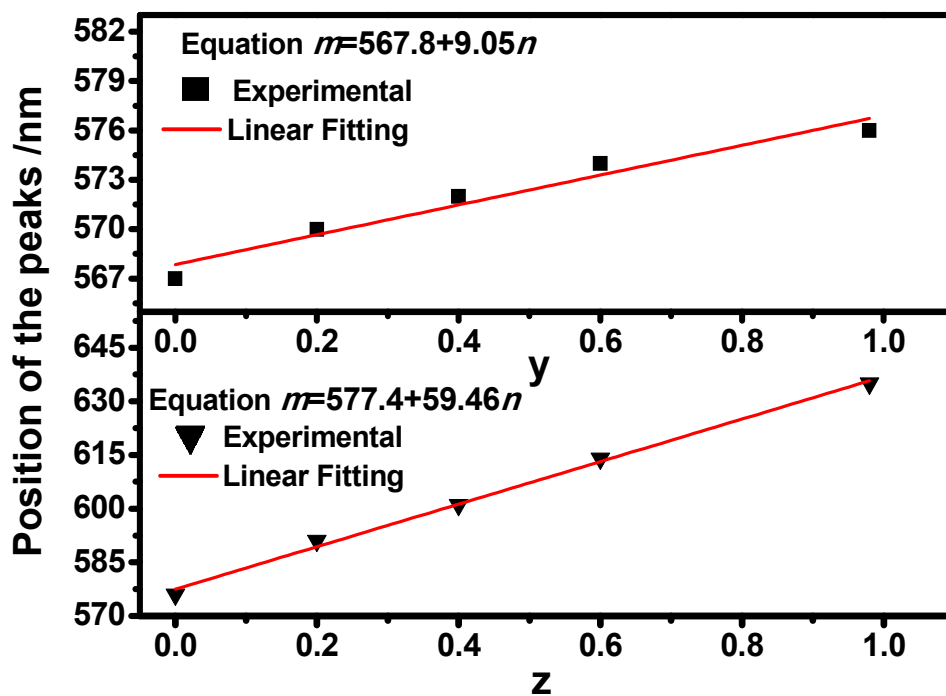


Fig. 4 (b)

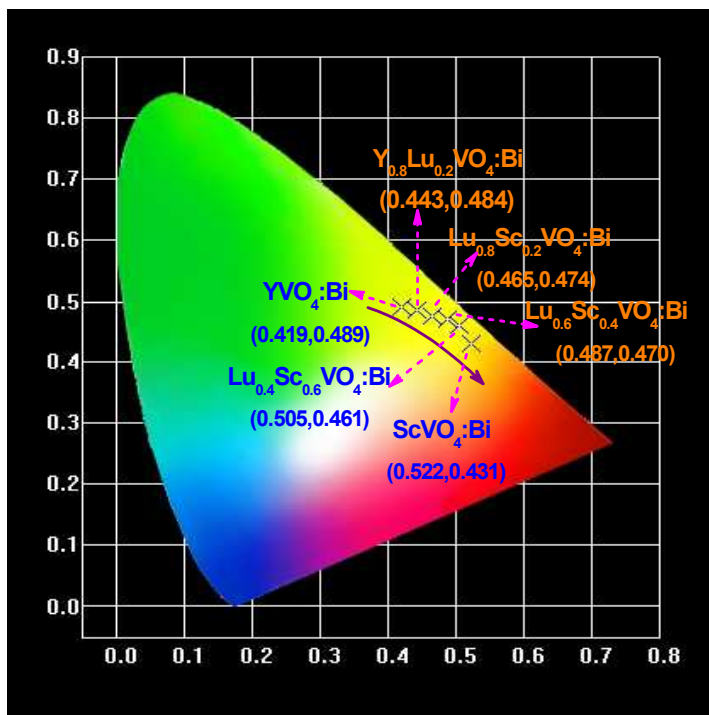


Fig. 4 (c)

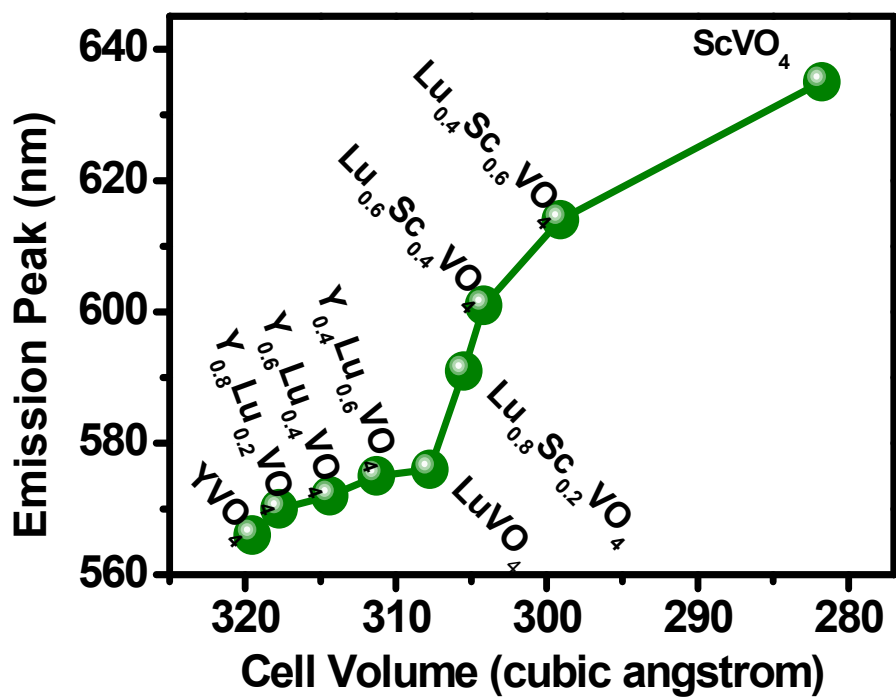


Fig. 4 (d)

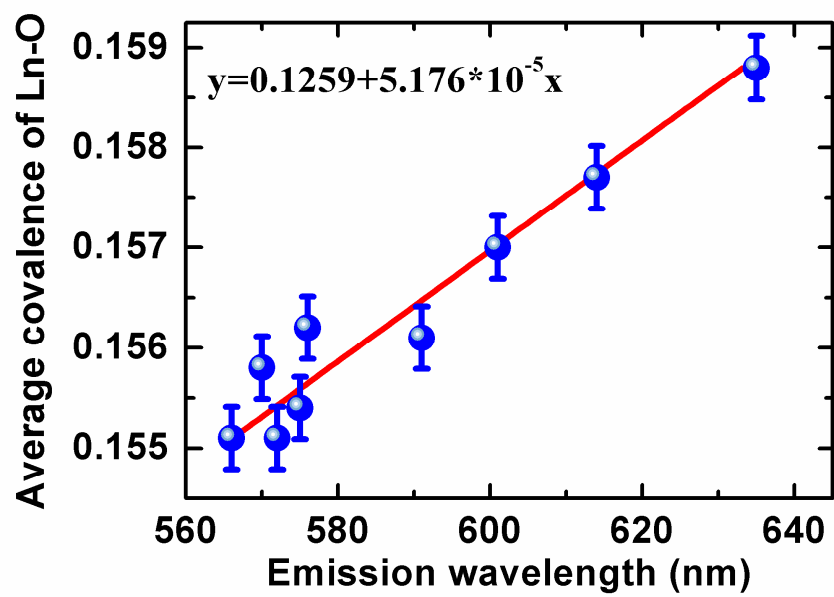


Fig. 5

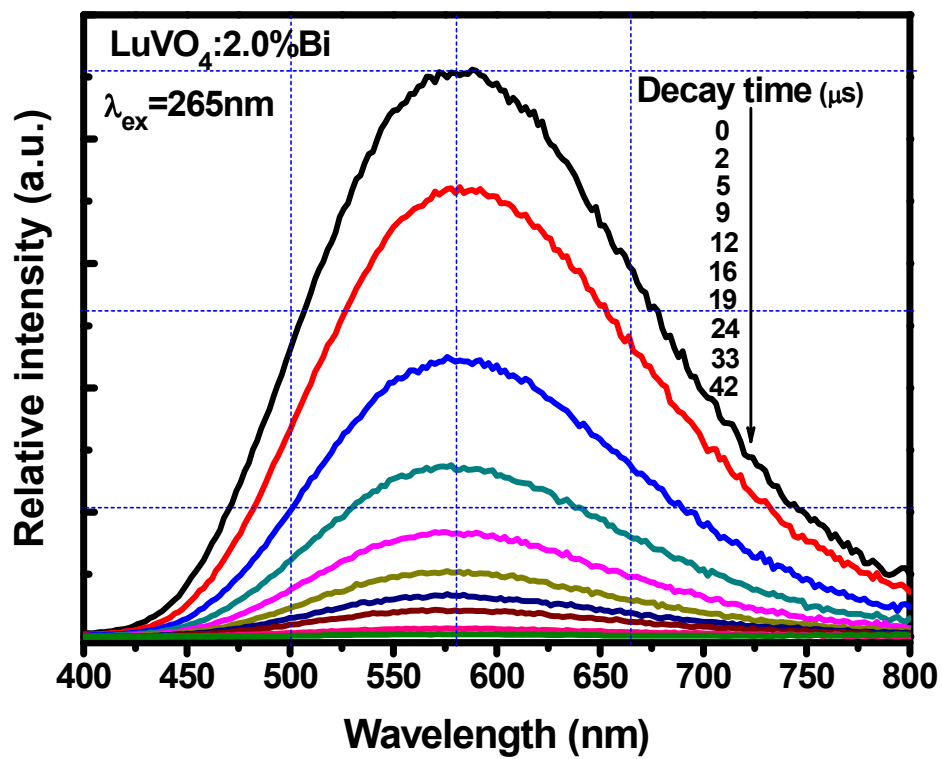


Fig.6

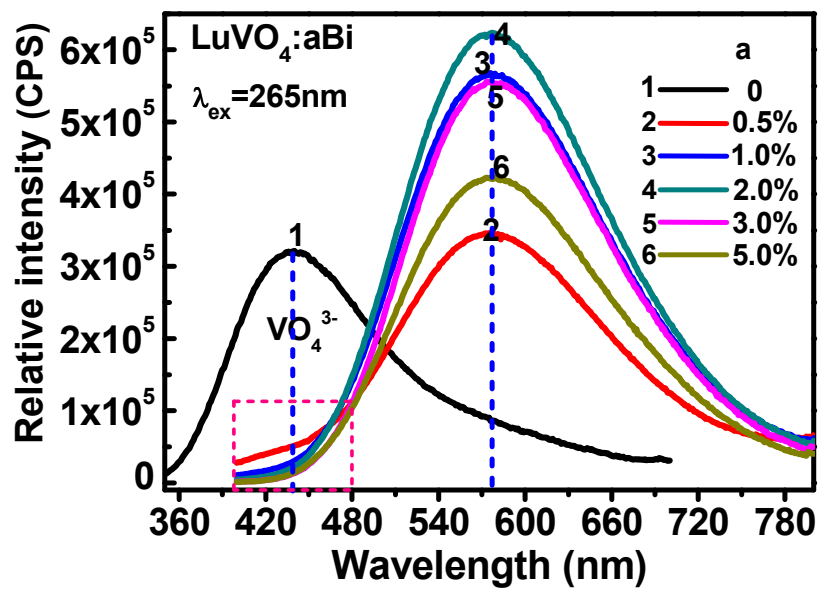


Fig.7

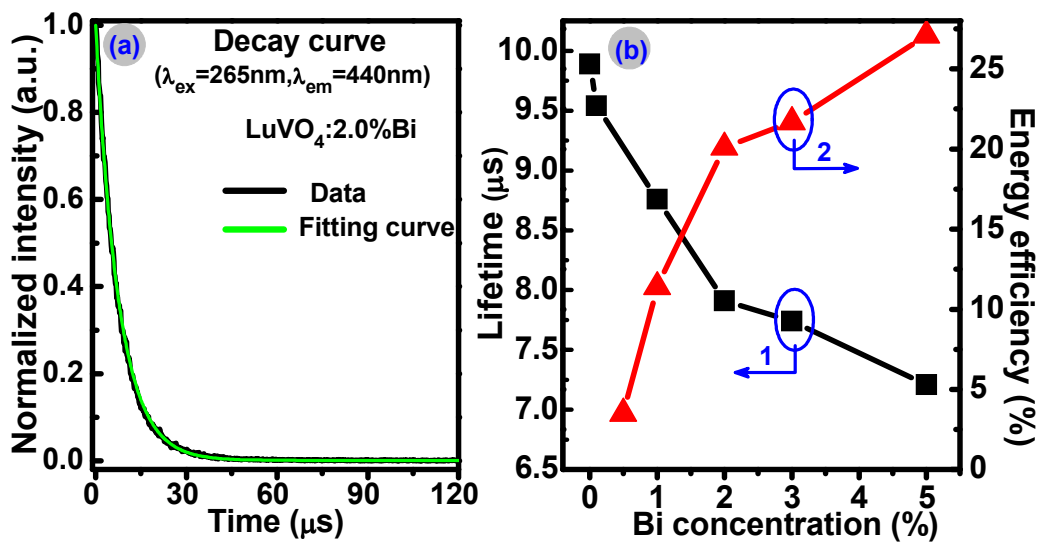


Fig.8

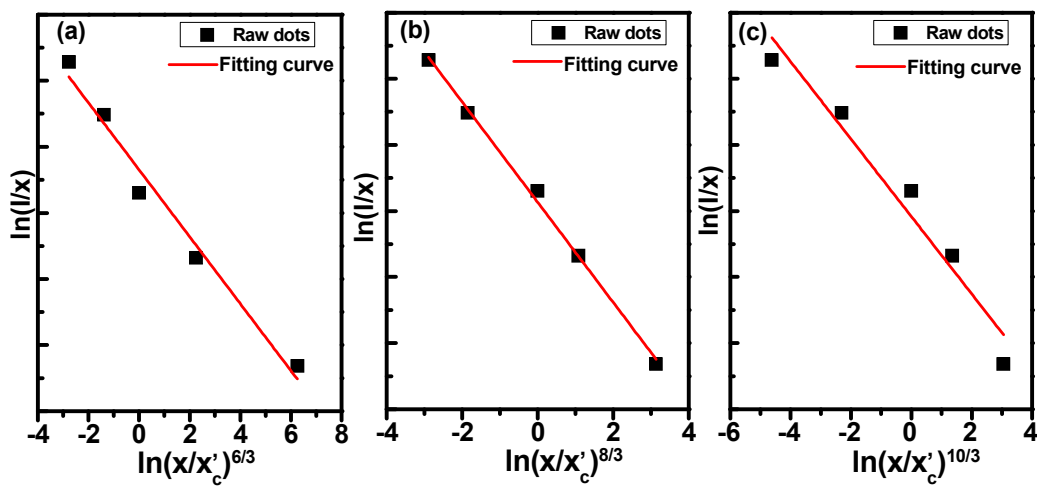
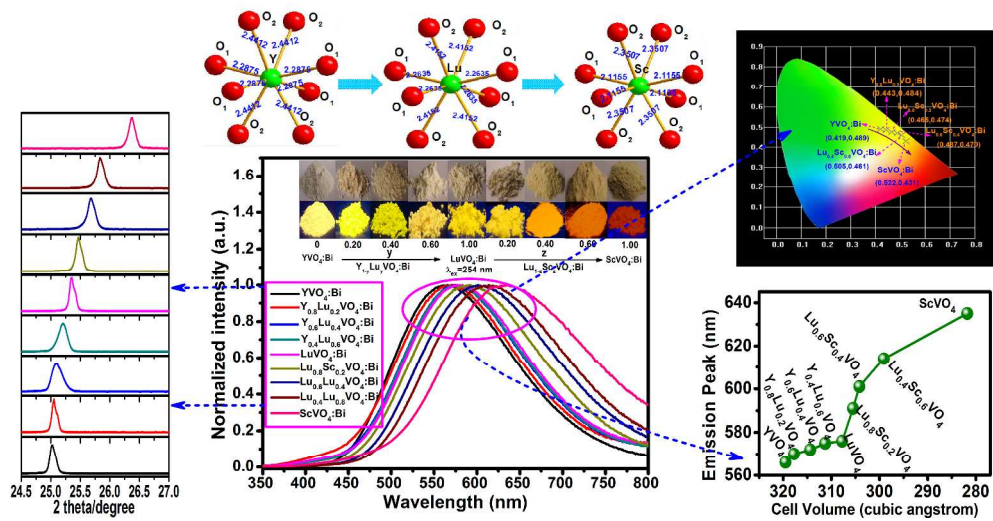


Fig.9



457x254mm (300 x 300 DPI)